

Ammonia, carbon dioxide and the non-detection of the 2152 cm⁻¹ CO band

Jiao He^{1,4}, Giulia Perotti¹, Shahnewaz M. Emtiaz², Francis E. Toriello², Adwin Boogert³, Thomas Henning¹, and Gianfranco Vidali²

¹ Max Planck Institute for Astronomy, Königstuhl 17, D-69117 Heidelberg, Germany

² Physics Department, Syracuse University, Syracuse, NY 13244, USA

³ Institute for Astronomy, University of Hawai'i at Manoa, 2680 Woodlawn Drive, Honolulu, HI 96822–1839, USA

⁴ e-mail: he@mpia.de

October 28, 2022

ABSTRACT

Context. CO is one of the most abundant ice components on interstellar dust grains. When it is mixed with amorphous solid water (ASW) or located on its surface, an absorption band of CO at 2152 cm⁻¹ is always present in laboratory measurements. This spectral feature is attributed to the interaction of CO with dangling-OH bonds (dOH) in ASW. However, this band is absent in observational spectra of interstellar ices. This raises the question whether CO forms a relatively pure layer on top of ASW or is in close contact with ASW, but not via dangling bonds.

Aims. We aim to determine whether the incorporation of NH₃ or CO₂ into ASW blocks the dOH and therefore reduces the 2152 cm⁻¹ band.

Methods. We performed laboratory experiments to simulate the layered structure of the ice mantle, that is, we grew CO ice on top of 1) pure ASW, 2) NH₃:H₂O=10:100 mixed ice, and 3) CO₂:H₂O=20:100 mixed ice. Infrared spectra were measured to quantify the strength of the 2152 cm⁻¹ band. In addition, a second set of experiments were performed to determine how the incorporation of NH₃ into ASW affects the dOH band.

Results. We found that annealing the ice reduces the 2152 cm⁻¹ band and that NH₃ blocks the dOH on ASW surface and therefore reduces the 2152 cm⁻¹ band more effectively than CO₂. We suggest that this difference between NH₃ and CO₂ can be ascribed to the polarity of the guest molecule (NH₃ is a polar species, whereas CO₂ is apolar). The polarity implies that the formation of an H-bond between the N atom of ammonia and the dOH is a barrier-less reaction. We also determined the pore surface area of the ice mixtures as a function of the annealing temperature, and found that the nondetection of 2152 cm⁻¹ band does not necessarily exclude the possibility of a porous ice mantle.

Key words. astrochemistry – Methods: laboratory: solid state – ISM: molecules – Solid state: volatile

1. Introduction

The nondetection of the 2152 cm⁻¹ (4.647 μm) band in astronomical observations of interstellar ices is one of the long-standing puzzles of astrochemistry. The 2152 cm⁻¹ band is the result of the interaction between absorbed CO and dangling-OH bonds (dOH) on amorphous water-ice surfaces (Sandford et al. 1988; Buch & Devlin 1991; Devlin 1992; Palumbo & Strazzulla 1992; Palumbo 1997; Collings et al. 2003a; Al-Halabi et al. 2004; Palumbo et al. 2010; He et al. 2019). This feature has been identified in laboratory CO:H₂O ice mixtures, whereas it appears to be absent in observational spectra of interstellar ices. The question then is why CO molecules apparently do not bind to the dangling-OH site in pre- and protostellar environments, resulting in spectra lacking the 2152 cm⁻¹ band.

At first, the nondetection was attributed to the low signal-to-noise ratio of observations in the 4 μm region, and thus, to the difficulties in resolving this band when the abundance of the responsible interstellar molecules is too low (e.g., Sandford et al. 1988; Ehrenfreund et al. 1997). A second explanation ascribed the nondetection to the low spectral resolution of the observations because of the overlap of several bands in the 4 μm region, such as gas-phase CO rovibrational transitions, the H₂ Pfund-β

emission line at ~2149 cm⁻¹ (Pontoppidan et al. 2002), and the C–N stretching mode at 2165 cm⁻¹ (Schmitt et al. 1989; Schutte & Greenberg 1997; Pendleton et al. 1999; Novozamsky et al. 2001).

With the advent of higher-resolution ground-based infrared instrumentation, it has been possible to disentangle the spectral features in the 4 μm region. In particular, the CO ice band was successfully resolved toward a sample of 39 low- to high-mass young stellar objects (YSOs) using the Very Large Telescope Infrared Spectrometer And Array Camera (VLT-ISAAC; Pontoppidan et al. 2003). In the VLT-ISAAC 3 – 5 μm survey the 2152 cm⁻¹ feature was not detected toward any source, and only stringent upper limits were provided (Pontoppidan et al. 2003). The large sample size (i.e., 39 objects), high signal-to-noise ratio, and spectral resolution of this set of observations suggested that the nondetection of the 2152 cm⁻¹ band is not linked to the capabilities of existing infrared facilities, but might be linked to the structure and composition of interstellar ices. It is well established that water-based ices in the interstellar medium (ISM) are amorphous, and a good analog of them is amorphous solid water (ASW). ASW grown by vapor deposition at low temperatures (~10–20 K) in the laboratory is highly porous with a very large specific surface area (Stevenson et al. 1999; Kimmel et al.

2001; Ayotte et al. 2001; He et al. 2019). As the temperature becomes higher, the porosity decreases, and the crystallinity increases. The blue wing of the broad OH-stretching absorption peak in the infrared contains two weak dOH absorption features at 3696 and 3720 cm^{-1} (Rowland et al. 1991; Buch & Devlin 1991; Palumbo 2005; Raut et al. 2007a; Palumbo et al. 2010; Dartois et al. 2013; Bu et al. 2015; He et al. 2019), which are attributed to 3- and 2-coordinated water sites on the pore surface, respectively. It has been demonstrated that the 3720 cm^{-1} (2.688 μm) feature is unstable and diminishes when the ASW is slightly annealed or exposed to irradiation (e.g., Palumbo 2005; Raut et al. 2007b; Bu et al. 2015; He et al. 2019), while the 3696 cm^{-1} (2.705 μm) feature persists even when the ASW is annealed to as high as 130 K. The more stable 3696 cm^{-1} feature was searched for in the ISM, but was not found (Keane et al. 2001). It is known that the 2152 cm^{-1} feature is linked to the interaction of CO with dOH (Devlin 1992), and that there is an anticorrelation between the 2152 cm^{-1} and 3696 cm^{-1} bands (He et al. 2019). Therefore, a theory that explains the nondetection of 2152 cm^{-1} feature when CO is present in the ice should also explain the nondetection of 3696 cm^{-1} when CO is absent.

Several laboratory studies have been devoted to studying the structure of water ice (porosity, pore surface area, etc.) and the dOH bonds, particularly the impact of energetic particles. Raut et al. (2007b) used 100 keV Ar ions to bombard ASW and found compaction of the ice and a decrease in the dOH peak area. They proposed that impacts from cosmic rays can explain the absence of dOH features in molecular clouds. Palumbo et al. (2010) used keV ions as well as Lyman-alpha photons (UV) to irradiate water-containing ices, and found that both UV and ions reduce the dOH band area and thus help to explain the nondetection of dOH feature. Dartois et al. (2013) used ions of even higher energy (MeV to GeV) to better simulate the effect of cosmic-ray bombardment and confirmed the compaction of ASW and the elimination of dOH bonds by ions. Behr et al. (2020) varied the temperature of ASW between 10 and 90 K and found that the decrease in dOH band area occurs in the whole temperature range they explored. These experimental works mostly focused on the ~ 3700 cm^{-1} dOH feature, but not directly on the 2152 cm^{-1} feature. All of these experimental studies indicate that energetic particles can make porous ASW compact and reduce the dOH feature. However, the compaction of pure ASW by either thermal processing or bombardment of energetic particles is unlikely to fully eliminate the dOH feature because the dOH feature in pure water ice is directly linked to its (pore) surface area. It has been found that regardless of whether the water ice is amorphous or crystalline, dOH is always present (Zhang & Buch 1990b,a; Rowland et al. 1991; Devlin 1992). The ice mantle might possess a certain level of porosity while at the same time the dOH feature is negligible. The dOH bonds might also be blocked by other molecules. We try to address these issues in the current study.

The answer to the nondetection of the 2152 cm^{-1} band was also directly investigated with laboratory experiments. Palumbo (1997) measured the infrared spectra of $\text{H}_2\text{O}:\text{CO}$ ice mixtures of different mixing ratios and compared the area of the two peaks at 2139 and 2152 cm^{-1} . She found that as the concentration of CO decreases, the 2152 cm^{-1} is more pronounced, suggesting that CO favors the dOH binding sites over other sites. Fraser et al. (2004) carried out experiments of layered $\text{CO}:\text{H}_2\text{O}$ ices with different CO coverage. The authors inferred that layered $\text{CO}:\text{H}_2\text{O}$ ices, with significant CO, are good interstellar-ice analogs over mixed ices because the 2152 cm^{-1} feature is not evident in their spectra. This is explained by the fact that CO can only react with

a small surface area, resulting in a 2152 cm^{-1} band under the detection limit. In this case, the ASW on dust grains would have a relatively compact structure, and CO would easily form a pure layer on top of the water-dominated layer. However, it is unclear whether the water-dominated layer is fully compact. The absence of 2152 cm^{-1} peak is unlikely to be explained by a compact ASW structure alone. For example, He et al. (2019) showed (see Fig. 9 in that paper) that CO on an ASW that was annealed to 140 K and cooled down to 20 K still has the 2152 cm^{-1} peak. For CO on pure ASW, the 2152 cm^{-1} peak is proportional to the surface area of the ASW (He et al. 2019). Even when we assume that all the interstellar water ice is fully compact, the surface area could still be significant, considering that dust grains could be fluffy. As an alternative explanation, Fraser et al. (2004) further speculated that some species other than CO, in particular, CO_2 , NH_3 , CH_4 , and CH_3OH , could adsorb at dangling-OH binding sites, thus removing the 2152 cm^{-1} feature in observational spectra. In this scenario, the ASW is still allowed to have a large surface area. However, Fraser et al. (2004) did not provide experimental confirmation of which interstellar ice components can act as effective dOH blockers.

Cuppen et al. (2011) tested this hypothesis by performing a spectroscopic study of $\text{CO}:\text{H}_2\text{O}:\text{CO}_2$ and $\text{CH}_3\text{OH}:\text{CO}$ mixtures. They found that a $\text{CH}_3\text{OH}:\text{CO}$ 1:1 mixture is sufficient to reproduce the observed width and peak position of the red component of the CO band, as well as the nondetection of the 2152 cm^{-1} band. In this regard, $\text{CH}_3\text{OH}:\text{CO}$ mixtures provided a better fit of one low-mass and one high-mass protostars over a $\text{H}_2\text{O}:\text{CO}$ mixture (Penteado et al. 2015). This finding suggested that CO might reside in H_2O -poor/ CH_3OH -rich environments in interstellar ices; this concept is supported by laboratory experiments and model simulations of CH_3OH formation from CO ice (Watanabe & Kouchi 2002; Fuchs et al. 2009; Cuppen et al. 2009).

Although convincing, a mixing ratio of $\text{CH}_3\text{OH}:\text{CO}$ 1:1 does not reflect the average composition of interstellar ices (Boogert et al. 2015). The $\text{CH}_3\text{OH}:\text{CO}$ ratio in high-mass YSOs is in fact subjected to large variations (0.2–3; Dartois et al. 1999; Boogert et al. 2002, 2008; Pontoppidan et al. 2003, 2008). In addition, for fewer than a handful of low-mass YSOs, the $\text{CH}_3\text{OH}:\text{CO}$ ratio is ≥ 0.7 (Pontoppidan et al. 2004; Perotti et al. 2020, 2021), and it is only 0.2–0.3 for starless and prestellar cores (Boogert et al. 2011; Chu et al. 2020; Goto et al. 2021).

Additionally, although it is plausible that a fraction of CO settles in CH_3OH -rich ices, a significant amount of it inevitably migrates and interacts with the H_2O matrix (Collings et al. 2003b; He et al. 2018b; Zamirri et al. 2018), contributing to the 2152 cm^{-1} band. This consideration is not taken into account in Cuppen et al. (2011) due to the selection of a $\text{CH}_3\text{OH}:\text{CO}$ mixture that does not contain H_2O . In summary, although large quantities of CH_3OH can act as a dangling-OH bond blocker, other more abundant species present in the ices, such as NH_3 and CO_2 , might also play a role in the suppression of the 2152 cm^{-1} band.

According to mid-infrared observations, the abundance of NH_3 ice in low- and high-mass star-forming regions is $\sim 5 - 7\%$ relative to H_2O (Dartois et al. 2002; Bottinelli et al. 2010; Öberg et al. 2011). However, laboratory constraints on optical constants and band strengths have shown that its abundance has been underestimated by up to 30% (Kerkhof et al. 1999; Zanchet et al. 2013). NH_3 is thought to form on the ice surface by the H-addition to N atoms (Hiraoka et al. 1995) while competing with the H-addition to O atoms. This suggests that NH_3 is formed simultaneously with water and is intimately mixed with water.

This might also result in newly formed NH₃ molecules reacting with dOH. Similarly, the abundance of CO₂ ice in the ISM has been estimated to be between 10 – 34% compared to H₂O (D’Hendecourt & Jourdain de Muizon 1989; de Graauw et al. 1996; Gibb et al. 2004; Pontoppidan et al. 2008; Noble et al. 2013). The most efficient formation pathways of CO₂ are proposed to be the reaction between CO and OH radicals (Noble et al. 2011; Oba et al. 2011; Ioppolo et al. 2011) or between CO and oxygen atoms (Roser et al. 2001). Because water is formed from O and OH as well, it follows that CO₂ should also be intimately mixed with water. It is possible that CO is binding to the dOH sites before forming CO₂, and therefore blocking the dOH sites (Fraser et al. 2004).

A related question that must be addressed is the quantification of the surface area of ices in the ISM. Ices play an important role in chemical reactions in the ISM because they provide a surface to adsorb and retain small reactive species, and because they stabilize reaction products by taking away the energy released in chemical reactions. The reaction rate depends on whether reactions occur in bulk ice or on the ice surface. The diffusion rate, which largely determines the rate of chemical reactions, is usually much faster on the surface than in bulk. When the chemistry in the ISM is modeled, it is necessary to distinguish surface reactions from reactions in bulk ice. For this reason, laboratory measurement of the surface area of astrophysically relevant ices provides key information for an accurate modeling of grain-surface reactions. As demonstrated by He et al. (2019), the pore surface area of ASW decreases with increasing annealing temperature, and the surface area is proportional to the band area of the 3696 cm⁻¹ dOH feature. It is therefore important to examine the pore surface area together with the dOH feature at 3696 cm⁻¹ or with the 2152 cm⁻¹ feature.

In the present paper, we test whether the absence of the 2152 cm⁻¹ feature is due to the interaction of CO with water ice and whether molecules such as NH₃ and CO₂ could block the dOH signatures of ASW. We performed a systematic study of different H₂O:NH₃ and H₂O:CO₂ ice mixtures, using porous ASW as the main ice analog component. CO was deposited on top of both mixtures. NH₃ and CO₂ were selected because they are ubiquitous species in astrophysical environments. In particular, they have been detected in the gas reservoirs of inner and outer regions of protoplanetary disks and in protostellar cores (Gürtler et al. 2002; Gibb et al. 2004; Öberg et al. 2010; Mandell et al. 2012; Salinas et al. 2016; Bosman et al. 2017; Pontoppidan et al. 2019; Najita et al. 2021) and on comets and planets (Mumma & Charnley 2011; Altwegg et al. 2020; Swain et al. 2008; Millan et al. 2021). This work focuses on the 2152 cm⁻¹ feature; we do not attempt to tackle the red component at ~2136 cm⁻¹. We do not compare the measured spectra with observations either because our measured spectra are in reflection mode, which should not be compared directly with observations.

This paper is structured as follows. We begin in Section 2 by describing the experimental setup used to record the laboratory spectra. In Section 3 we test the effectiveness of CO₂ and NH₃ as dOH bond blockers and present the key experimental results. Section 4 discusses the results and explains them by comparing the chemical behaviors of CO₂ and NH₃ embedded in H₂O. Additionally, it supplies a list of additional dOH-blocker candidates. We summarize our conclusions in Section 5.

2. Experimental setup

Experiments were performed using an ultra-high vacuum (UHV) chamber that has been described previously (He et al. 2018a,b,

2019). The main UHV chamber was pumped to a base pressure of 4×10^{-10} Torr when the cryostat was off. A gold-coated copper disk was used as the substrate onto which ice samples were grown. The temperature of the substrate can be controlled between 5 and 400 K by using a closed-cycle helium cryostat and a cartridge heater installed right underneath the substrate. The temperature was measured using a calibrated silicon diode sensor to an accuracy of 0.05 K. Gas or vapor was deposited through one of the two UHV variable leak valves, which were controlled by stepper motors interfaced to a computer. A LabVIEW program automates the gas and vapor deposition and calculates the thickness in real-time. A more detailed description of the gas deposition is given in the Appendix of He et al. (2018a). Although the UHV system is equipped with two highly collimated molecular beam lines for gas deposition, we only used the leak valves because the background deposition from leak valves is a better simulation of the omnidirectional deposition of gases in interstellar space. Water vapor was evaporated from distilled water, which underwent at least three freeze-pump-thaw cycles to remove dissolved air. Ice samples were analyzed by a Nicolet 6700 Fourier Transform InfraRed (FTIR) Spectrometer in the reflection absorption infrared spectroscopy (RAIRS) configuration. Infrared spectra were obtained by averaging eight scans every 10 seconds in the range 650–4000 cm⁻¹. The infrared beam is at a 78 ° incidence angle relative to the surface normal. In this reflection mode, the infrared band profile may differ from the transmission mode, such as that in Cuppen et al. (2011). Particularly, the longitudinal optical (LO) mode of CO at 2143 cm⁻¹, which appears when the coverage of CO on the surface is relatively high, is only present in reflection mode. In this study, we mostly focus on the relatively weak dOH features at low coverage of CO. Here the difference between reflection and transmission geometry is not important.

3. Experimental results and analysis

3.1. CO deposition on water-dominated ice mixtures

Two sets of experiments were performed in the current study; they are described in this subsection and Sect. 3.2. The first set is an extension to the experiments reported in He et al. (2019). He et al. (2019) grew 200 monolayers (ML; defined as 10^{15} molecule·cm⁻²) of water by vapor condensation on the gold surface with the surface at 10 K. At this temperature, the water ice is amorphous and highly porous. Afterward, the water ice was warmed up to an annealing temperature T_{ann} and remained at this temperature for 30 minutes to stabilize the ice structure. The following annealing temperatures were chosen: $T_{\text{ann}} = 20, 40, 60, 80, 100,$ and 120 K. After annealing, the ice was cooled down to 20 K before depositing CO on top of the water ice, and RAIRS spectra were collected during the CO deposition. We chose to make a layered ice rather than a uniformly mixed one to better represent the layered ice mantle on dust grains (Pontoppidan et al. 2008; Boogert et al. 2015). This is different from other studies, in which gases were premixed and then deposited (e.g., Ehrenfreund et al. 1997; Cuppen et al. 2011). In addition to the experiments in He et al. (2019), in the present study, we replaced pure water with (1) mixed ice of 200 ML H₂O and 20 ML NH₃ or (2) mixed ice of 200 ML H₂O and 40 ML CO₂. The ratios CO₂:H₂O and NH₃:H₂O are representative of that in the ice mantle on dust grains (Pontoppidan et al. 2008; Öberg et al. 2011; Zanchet et al. 2013; Boogert et al. 2015). Other than the difference in ice composition, the experiments follow the same procedure as in He et al. (2019). The deposition of H₂O:CO₂

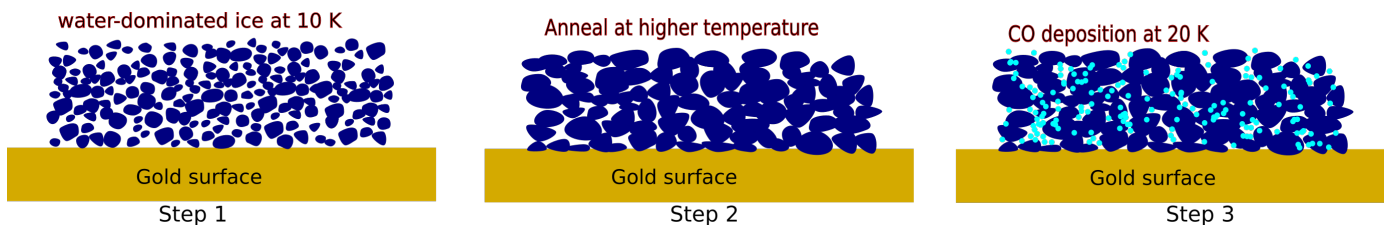


Fig. 1. Cartoon of the procedure of the first set of experiments. Step 1: Water-dominated ice was deposited at 10 K, forming a highly porous amorphous ice. Three different ice compositions were chosen: (1) 200 ML H₂O, (2) mixture of 200 ML H₂O and 20 ML NH₃, and (3) mixture of 200 ML H₂O and 40 ML CO₂. Step 2: Ice was warmed up to a higher temperature to anneal for 30 minutes. The following temperatures were chosen: 20, 40, 60, 80, 100, or 120 K. Step 3: Ice was cooled down to 20 K and exposed to CO deposition. RAIRS spectra were recorded during the CO deposition, which is shown in Fig. 2.

and H₂O:NH₃ ice mixtures was accomplished by codeposition of the two gas and vapor components within 20 minutes and 25 minutes, respectively. Fig. 1 demonstrates the procedure of the experiments. RAIRS spectra were measured during CO deposition on ices, a selection of which is shown in Fig. 2.

It has been shown that CO molecules can diffuse and penetrate porous ASW already at below 16-20 K, reaching all the surface area pores (Mispelaer et al. 2013; Karssemeijer & Cuppen 2014; Lauck et al. 2015; He et al. 2018b, 2019). The same is true in the H₂O:CO₂ and H₂O:NH₃ mixtures. The second and third columns of Fig. 2 show that when the CO coverage is below saturation of the surface, the peak profile is similar to the profile that is usually seen in CO and H₂O mixed ice. At the beginning of the CO deposition, the coverage of CO on the pore surface is small, and all the CO molecules interact with the water surface, which is shown by the two peaks in the infrared centered at ~ 2139 and ~ 2152 cm⁻¹. As CO gas deposition proceeds, the pore surface area is gradually covered by CO, and eventually, CO builds up as pure CO ice; at this stage, CO primarily interacts with other CO molecules rather than with the water surface. This is indicated by the emergence of a 2143 cm⁻¹ absorption peak due to the LO mode of CO. Similar to He et al. (2019), we took the CO deposition amount at which the 2143 cm⁻¹ peak emerges as the pore surface area of the ASW. Fig. 3 shows the pore surface area, in units of ML, of the three ices at different annealing temperatures. The error bar accounts for the uncertainty in determining the emergence of the LO peak. The introduction of 20% CO₂ into water ice lowers the pore surface area by almost half, while 10% of NH₃ has only a small impact on the surface area. One possible reason why CO₂ more effectively blocks the pore surface area is that CO₂ forms clusters on the surface of ASW (He et al. 2017), which block some micropores.

The band area of the 2152 cm⁻¹ peak in Fig. 2 can also be analyzed. By visual inspection, we can see that the peak area decreases at higher annealing temperatures for all three ices. When annealed at 120 K, the 2152 cm⁻¹ peak becomes insignificant. In H₂O:NH₃ mixtures, the decrease in 2152 cm⁻¹ peak area is more pronounced. Even if the annealing temperature is only 60 K, the 2152 cm⁻¹ peak appears to be the tail of the 2143 cm⁻¹ peak rather than a separate peak. When the H₂O:NH₃ mixture is annealed to 100 K, the 2152 cm⁻¹ peak disappears almost completely, while in the H₂O:CO₂ mixture, the 2152 cm⁻¹ peak is still significant. Fig. 4 shows a zoom-in of the fifth row of Fig. 2, corresponding to the ices annealed to 100 K. Because the 2152 cm⁻¹ peak is directly correlated to CO interacting with the dOH bonds (He et al. 2019), it is evident that 10% of NH₃ blocks the dOH bonds more effectively than 20% of CO₂, provided that the ice is annealed to higher than 80 K. As discussed above, 20% of CO₂ reduces the surface area of ASW by half, which should also reduce the dOH sites proportionally. In the CO₂:H₂O mixture we

note that the surface area decreases to half throughout the experiment (Fig. 3), but in contrast to expectations, the 2152 cm⁻¹ peak is not equally reduced to half. This observation strengthens the argument that CO₂ is a less efficient dOH blocker.

To quantify it, we calculated the 2152 cm⁻¹ peak area by using the sum of two Gaussian functions to fit the spectra in Fig. 2. Because the 2143 cm⁻¹ peak only emerges after the surface is saturated by CO, that is, the 2152 cm⁻¹ peak is saturated before the emergence of the 2143 cm⁻¹ peak, we only focused on the spectra before the emergence of the 2143 cm⁻¹ peak. The advantage is that we only need two components for the fitting. Fig. 5 shows examples of the fitting. With a small amount of CO on the surface, the fitting by the sum of two Gaussian functions is excellent. However, after CO fully covers the surface, the fitting becomes worse, as illustrated by the top trace in the left panel. This is also demonstrated in the right panel. As the surface is fully covered by CO, the error bar of the 2152 cm⁻¹ band area becomes very large. From the right panel, we can determine the saturation 2152 cm⁻¹ peak areas. This analysis procedure is repeated for the ices with different annealing temperatures, and the results are shown in Fig. 6. Here we can see that 10% of NH₃ effectively blocks the dangling OH bonds as long as the ice mixture is annealed to 100 K. We note that the fitting only calculates the area of the 2152 cm⁻¹ peak, but does not consider its shape. For H₂O:NH₃ mixtures annealed to 60 K and above, the 2152 cm⁻¹ component looks as if it is the tail of the 2140/2143 cm⁻¹ peak rather than a separate peak, making it more difficult to discern than for H₂O:CO₂ mixtures in astronomical observations.

Introducing CO₂/NH₃ into ASW has an impact on both the pore surface area and the fraction of dOH sites on the pore surface. It is necessary to determine whether the decrease of dOH is due to the blocking by CO₂/NH₃ or due to the decrease of the pore surface area. For this reason, the saturation band area for the 2152 cm⁻¹ band in Fig. 6 was divided by the pore surface area in Fig. 3 to obtain the normalized dOH blocking efficiency. The result is shown in Fig. 7. NH₃ lowers the 2152 cm⁻¹ band area per pore surface area compared with pure ASW. In contrast, CO₂ even increases the 2152 band area per pore surface area because it reduces the pore surface area more effectively. This confirms that NH₃ is an effective dOH blocker on ASW surface.

3.2. Dangling-OH bonds in H₂O:NH₃ ice mixtures

The results of the first set of experiments presented above suggest that introducing NH₃ into water-dominated ice can effectively decrease the 2152 cm⁻¹ peak and that NH₃ is an effective dOH bond blocker. In the second set of experiments, we further explore how the concentration of NH₃ and the temperature

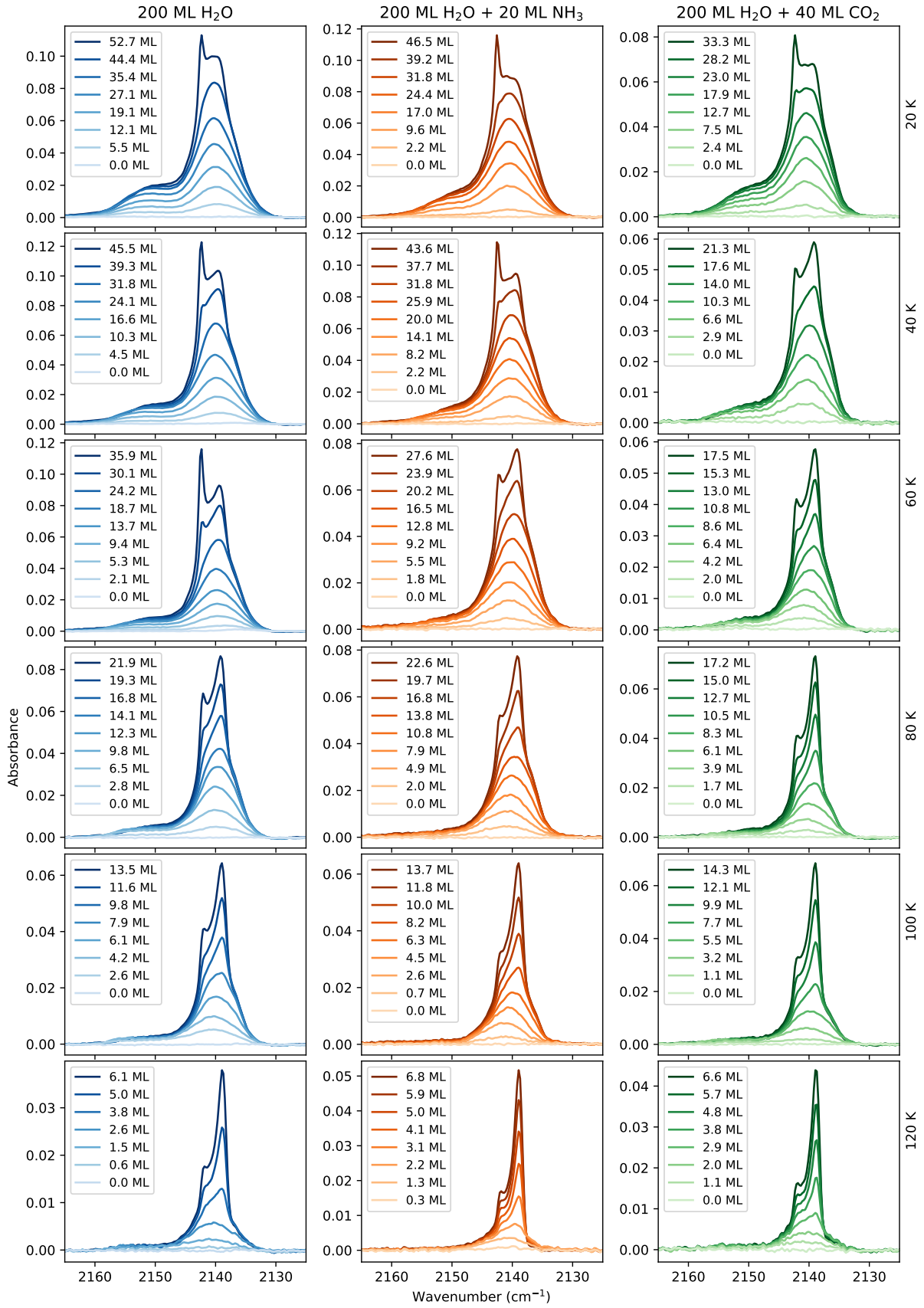


Fig. 2. Selected RAIRS spectra of CO deposited on water-dominated ice after the ice was annealed to temperature T_{ann} and then cooled to 20 K. T_{ann} is 20, 40, 60, 80, 100, and 120 K from top to bottom. The three columns are for (1) 200 ML of pure H₂O ices, (2) mixed ices of 200 ML H₂O and 20 ML NH₃, and (3) mixed ices of 200 ML H₂O and 40 ML CO₂. The insets of the figure refer to the amount of deposited CO.

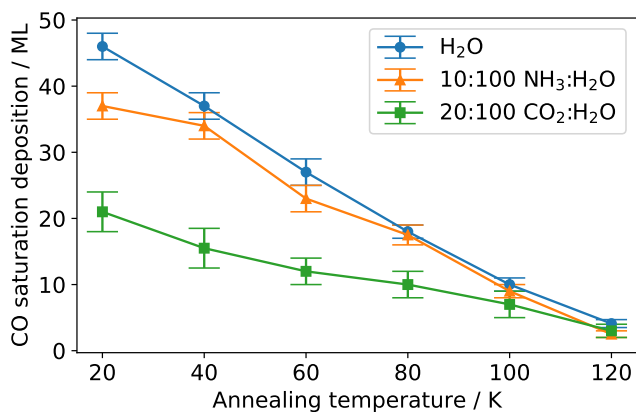


Fig. 3. Pore surface area of water-dominated ice (mixture) that is annealed to different temperatures, as determined from Fig. 2. The surface area is the CO deposition dose at which the 2143 cm^{-1} peak emerges.

of the ice affect the dOH bonds. We fixed the amount of water to be 100 ML, and deposited $\text{NH}_3:\text{H}_2\text{O}$ ice mixtures with mixing ratios ranging from 0:100 to 30:100. After the deposition of the mixture at 10 K, the ice was warmed up at a ramp rate of 6 K/minute, and RAIRS spectra were collected.

The spectra of ice with mixing ratio of $\text{NH}_3:\text{H}_2\text{O}=0:100$, 10:100, and 20:100 during warm-up are shown in Fig. 8. In pure water ice, both the dOH bands at 3696 and 3720 cm^{-1} are present at the lowest temperature. The 3720 cm^{-1} band disappears by about 60 K, and the 3696 cm^{-1} band persists until above 120 K. For a more detailed discussion of the dOH bands of pure ASW, see He et al. (2019). When 10% or 20% of NH_3 is added to the mixture, the 3720 cm^{-1} peak is indiscernible, except for the 10% mixture at the lowest temperature. The 3696 cm^{-1} peak is much lower than that for pure ASW, particularly when the ice mixture is warmed up.

Following a similar method as in He et al. (2019), we calculated the area for the 3696 cm^{-1} peak. A broad Gaussian function was used to fit the blue wing of the OH-stretch peak, and two narrow Gaussian functions were used to fit the peaks at 3696 and 3720 cm^{-1} . The band area of the 3696 cm^{-1} peak was obtained from the fitting. The results are shown in Fig. 9. With an $\text{NH}_3:\text{H}_2\text{O}$ mixing ratio between 0 and 15%, the dOH band area decreases with increasing NH_3 concentration at all temperatures. At higher mixing ratios, the dOH band area becomes less dependent on the concentration. When the mixing ratio is higher than 10%, the dOH band is almost negligible when annealed to 100 K or above. This agrees with the results of the 2152 cm^{-1} peak in Section 3.1. This is expected because it is known that the 2152 cm^{-1} peak is correlated with the dOH band at 3696 cm^{-1} (He et al. 2019).

3.3. $\text{H}_2\text{O}:\text{CO}_2$ ice mixtures

Similar experiments as in Section 3.2 might be performed for $\text{CO}_2:\text{H}_2\text{O}$ mixtures, and the dOH region might be monitored in the infrared. Such experiments have already been performed and presented in Figure 3 of He et al. (2018a). The dOH bonds of water are shadowed by the $\nu_1 + \nu_3$ combination mode, and therefore it is challenging to analyze the dOH at 3696 cm^{-1} similar to that in Section 3.2. Previously, Cuppen et al. (2011) measured the infrared spectra of $\text{H}_2\text{O}:\text{CO}:\text{CO}_2$ mixtures, and found that it takes a large amount of CO_2 to suppress the 2152 cm^{-1} band at low tem-

peratures. Even with a mixture of $\text{H}_2\text{O}:\text{CO}:\text{CO}_2=2.75:1:10$, that is, three to four times more CO_2 than H_2O , there is still a non-negligible 2152 cm^{-1} peak. It is clear from both Cuppen et al. (2011) and this study that CO_2 is a less effective dOH blocker.

4. Discussion

4.1. The surface area and the nondetection of dOH bands

The porosity of the ice mantle covering dust grains in the ISM is still debated. Porous water ice provides a large catalytic surface area for grain surface reactions to take place, while reactions in compact ice are challenged by high-diffusion energy barriers for most particles inside bulk compact water ice. The detection of a large variety of complex organic molecules seems to favor the argument that the water-rich ice is somewhat porous and provides a large surface area. However, similarly to the 2152 cm^{-1} band, also the 3696 cm^{-1} dOH band, which is usually present in vapor deposited ASW, has never been detected in interstellar ices (Keane et al. 2001). This raises the questions why the dOH bands disappear, and whether there is a dOH blocker in the ice. Closely related is the nondetection of the 2152 cm^{-1} peak for CO ice on water surface.

Previous studies have found that energetic particles bombardment as well as thermal processing reduce the dOH bonds in ASW and make the ice more compact (e.g., Raut et al. 2007b; Palumbo 2006; Dartois et al. 2013; He et al. 2019, and references therein). There is also evidence that the ability of CO to diffuse into the ASW is affected by ion processing, which then reduces the 2152 cm^{-1} peak (Palumbo 1997). However, these previous studies did not explore the possibility of having a somewhat porous ice structure without the simultaneous presence of the 2152 cm^{-1} peak (or the 3696 cm^{-1} peak). Our study fills the gap and determines whether dOH might be blocked by other molecules in the ice. We determine whether the ice mantle covering dust grains can have an insignificant 2152 cm^{-1} peak (or equivalently, insignificant 3696 cm^{-1} dOH band), but still have a significant surface area. Figs. 3, 6, and 9 show that this is possible if 10% of NH_3 is mixed with water and the ice is annealed to 100 K (this is on the laboratory timescale, it will be lower on the timescale of a molecular cloud). In the ISM, ices are not condensed from gas and annealed like in the experiments, but are formed by chemical reactions on the surface. The energy released from chemical reactions can be absorbed by the ice and can create some localized “annealing”, which makes the ice less porous (Oba et al. 2009; Accolla et al. 2011). The bombardment of cosmic rays can also induce some local heating of ice and therefore change the ice structure (Palumbo 2006; Raut et al. 2007b; Dartois et al. 2013; Mejía et al. 2015; Behr et al. 2020). Eventually, the state of the ice might be similar to the ice that is condensed from gas and then annealed to a high temperature, such as 100 K. In this scenario, the 3696 cm^{-1} dOH peak or the 2152 cm^{-1} peak becomes negligible when ammonia is present. We speculate that this may explain the nondetection of these two features.

4.2. Effect of polarity on the nondetection of the dOH bands

The important question that arises after analyzing the different responses of $\text{H}_2\text{O}:\text{NH}_3$ and $\text{H}_2\text{O}:\text{CO}_2$ ice mixtures is what makes NH_3 a more effective dOH blocker than CO_2 . The answer to this question can be found by comparing the hydrophilicity and the chemical characteristics and behaviors of NH_3 and CO_2 .

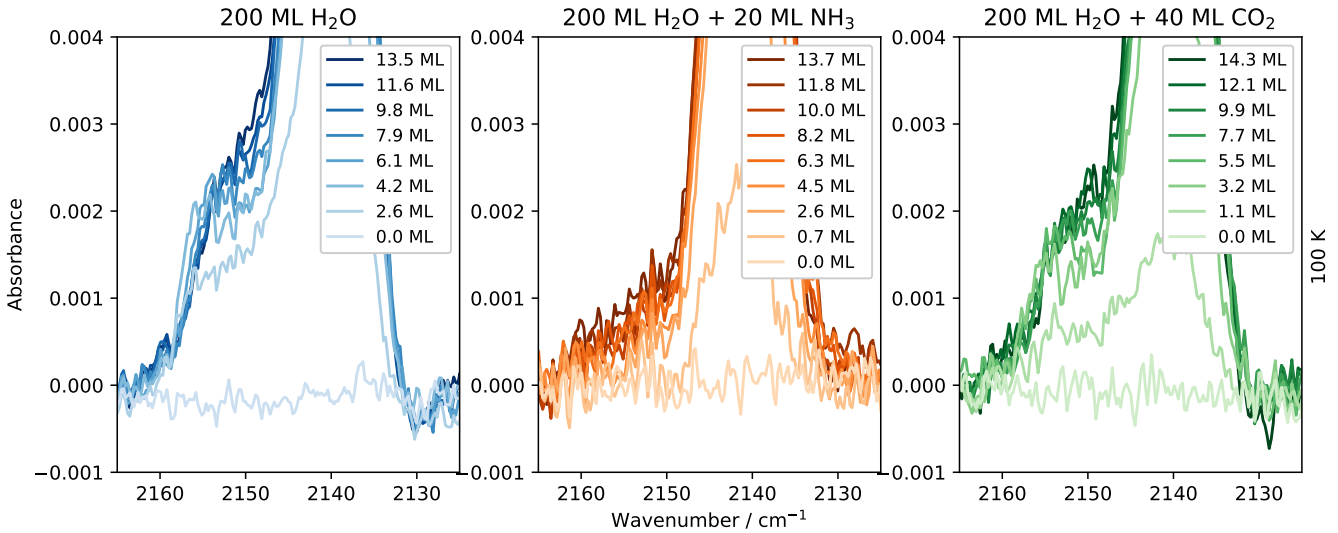


Fig. 4. Zoom of the fifth row (100 K) of Fig. 2.

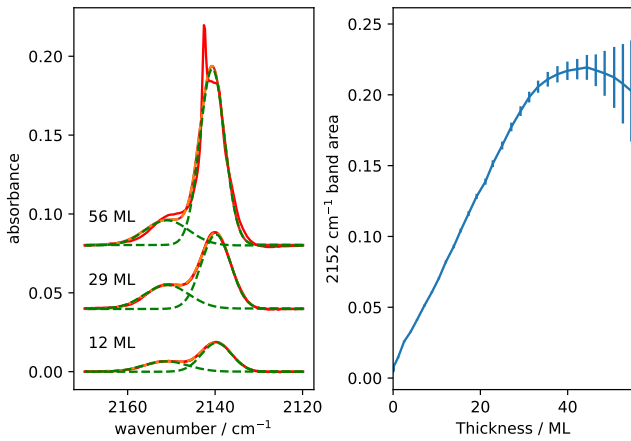


Fig. 5. Illustration of the method for determination of 2152 cm⁻¹ band area. Left panel: Examples of the fitting of the CO absorption profile using the sum of two Gaussian functions. The red lines are the measured spectra, the dashed green lines are the two Gaussian components, and the orange lines are the total fitting. Spectra are offset for clarity. Right panel: Band area of the 2152 cm⁻¹ component during CO deposition; the error bar of the fitting is also shown. The large error bar at larger thickness is due to the emergence of the LO peak at 2143 cm⁻¹.

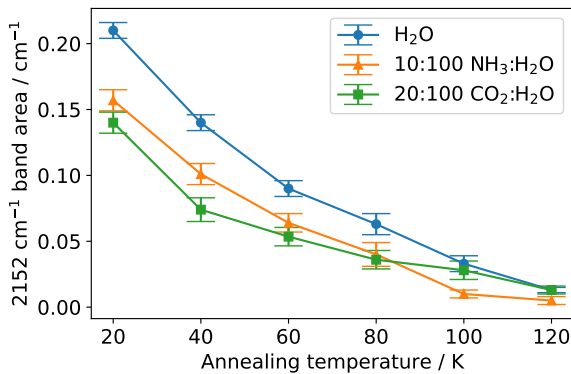


Fig. 6. Saturation band area for the 2152 cm⁻¹ band, as shown in Fig. 2. The band area is calculated by applying the fitting protocol illustrated in Fig. 5.

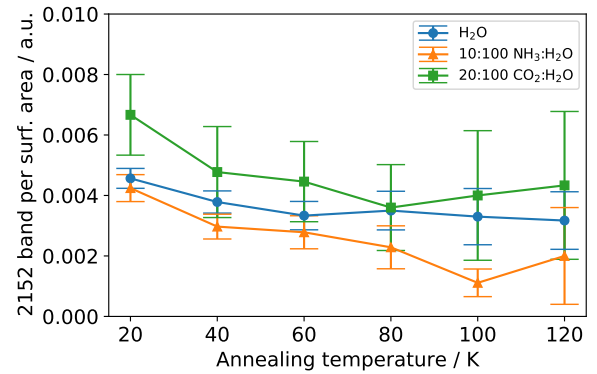


Fig. 7. Saturation band area for the 2152 cm⁻¹ band as shown in Fig. 6, divided by the pore surface area, as shown in Fig. 3.

The blocking of dOH bonds on deuterated ASW (d-ASW) has been studied by [Devlin \(1992\)](#). In this work, d-ASW was pre-covered with CF₄ or ethylene oxide, and then the infrared spectra of the dOH band at ~2730 cm⁻¹ and the band at 2152 cm⁻¹ were monitored to investigate the interaction of CO with dOH. [Devlin \(1992\)](#) found that precovering with CF₄ enhances the 2152 cm⁻¹ band, whereas precovering with ethylene oxide reduces it. This behavior was attributed to their hydrophilicity. CF₄ is a hydrophobic molecule and therefore avoids dOH bonds and associates strongly with surface oxygen. In contrast, ethylene oxide, as a hydrophilic molecule, primarily binds to surface hydrogen atoms that belong to OH groups, effectively decreasing the number of available dOH groups.

The current study investigates whether NH₃ and CO₂ block the dOH. NH₃ is a hydrophilic molecule such as ethylene oxide, which wets the whole ASW surface before building up as pure layers, as indicated from temperature programmed desorption (TPD) of NH₃ on water ice ([He et al. 2016](#)). In comparison, CO₂ is hydrophobic, and it forms clusters on ASW surface before the whole surface is covered. The TPDs of CO₂ also show that the interaction force between CO₂ and CO₂ is stronger than that between CO₂ and H₂O ([He et al. 2018a](#)). This explains why NH₃ blocks dOH while CO₂ does not.

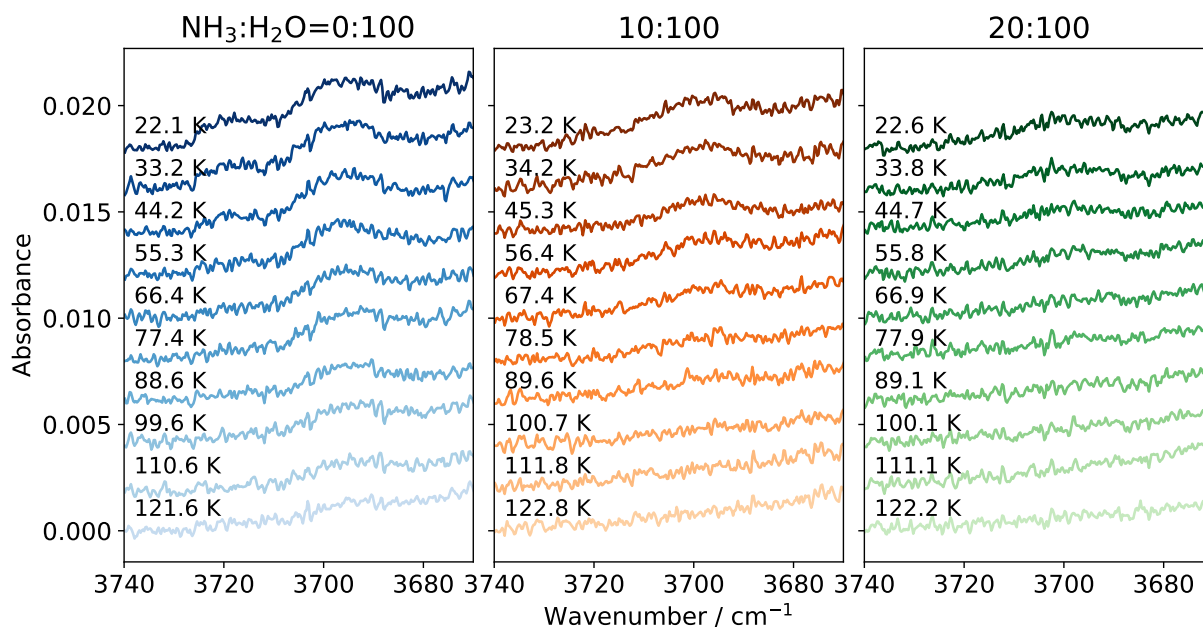


Fig. 8. Dangling-OH bond region of the RAIRS spectra for $\text{NH}_3:\text{H}_2\text{O}$ mixtures during warming up. The mixing ratios and temperatures are indicated in the figure.

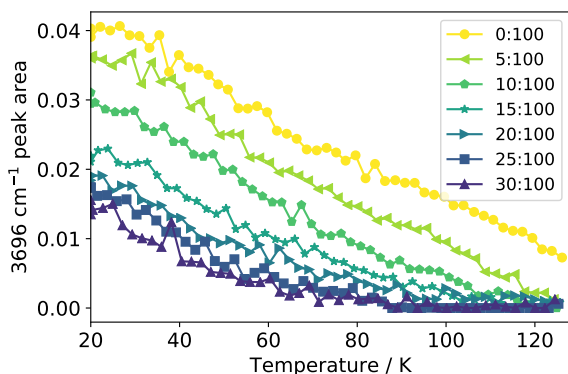


Fig. 9. Dangling-OH bond 3696 cm^{-1} band area in $\text{NH}_3:\text{H}_2\text{O}$ mixtures during warming up. The mixing ratios and temperatures are indicated in the figure.

We can also view it from a different aspect by examining their chemical characteristics. NH_3 and H_2O are structural analogs and isoelectronic species, as they possess the same number of electrons. Both species are nucleophiles: the O atom in H_2O and the N atom in NH_3 have two unpaired electrons, which can be donated to form hydrogen bonds. Most importantly, because they are characterized by an unequal sharing of valence electrons (i.e., a difference in electronegativity among the bonded atoms), NH_3 and H_2O are defined as polar. They have permanent dipole moments. In contrast, CO_2 is a linear molecule with an equal sharing of valence electrons, hence it is apolar. The fact that NH_3 is polar and CO_2 is apolar implies that NH_3 can bind more tightly to H_2O molecules compared to CO_2 , as confirmed by laboratory measurements using TPD (He et al. 2016, 2018a), which found that a low coverage of NH_3 desorbs from water ice at $\sim 140\text{ K}$, much higher than CO_2 , which desorbs at $\sim 80\text{ K}$. The binding energy on water ice was also studied using quantum chemistry calculations. Ferrero et al. (2020) modeled an interstellar ice surface by simulating both crystalline and

amorphous water ices with DFT (B3LYP-D3 and M06-2X). The authors of this work determined binding energies for 21 astrochemically relevant species. On ASW ices, they found that NH_3 has binding energy ranges from 4314 to 7549 K, which is several times higher than CO (1109–1869 K) and CO_2 (1489–2948 K), corroborating the strong binding between NH_3 and water found in experiments. This strong binding makes NH_3 a more effective dOH band blocker over CO_2 (Fig. 10).

Henkelman & Feibelman (2016) performed density functional theory (DFT) calculations of the interaction of NH_3 with the dOH of water ice and showed that the bond between ammonia and the dOH is promoted by the attraction of the lone pair of the N atom to the dOH of H_2O . This is a zero-energy barrier reaction that results in the formation of an $\text{OH}\cdots\text{NH}_3$ hydrogen bond. This theoretical study strongly supports laboratory results that proved that NH_3 flags the dOH binding sites (Lechner et al. 2015). Both studies revealed that the sole presence of an NH_3 molecule in the vicinity of H_2O molecules causes the latter to reorient with zero-energy barrier to expose a dOH bond toward the N atom of NH_3 .

This is not the case for apolar molecules such as CO or N_2 , which are not capable of binding as strongly as NH_3 to the dOH bonds. Consequently, because their attraction to dOH is weaker, their H-bonding with H_2O proceeds with nonzero energy barriers. The highest barrier and thus weakest binding to water is found for N_2 , followed by CO (Henkelman & Feibelman 2016). This implies lower probabilities for the adsorption of N_2 and CO at the dOH sites over NH_3 , and therefore less effective dOH blocking capabilities at the low temperatures of the interstellar medium (ISM). This result agrees with the inefficient dOH blocking behaviors of CO (Fraser et al. 2004) and CO_2 (this work and Cuppen et al. 2011).

Previous laboratory studies of the nondetection of the 2152 cm^{-1} band have proposed that good dOH blockers are species that form from CO molecules at the dOH sites (e.g., CO_2 and CH_3OH ; Fraser et al. 2004; Cuppen et al. 2011; see Section 4.3). By working with NH_3 and CO_2 , we have discovered that an important requirement for a good dOH-bond blocker is the po-

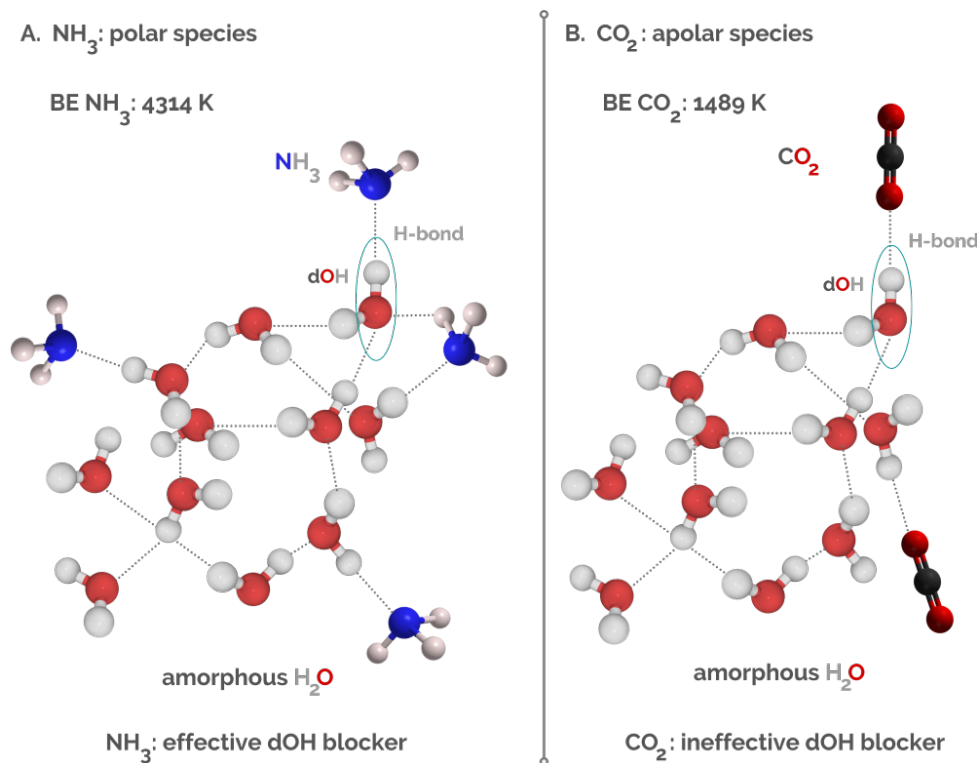


Fig. 10. Schematic illustration of the interactions between A) dOH and ammonia (NH₃) and B) dOH and carbon dioxide (CO₂). NH₃ is a polar molecule, it tightly binds to the dOH via H-bonding between the N atom and the dOH. CO₂ is an apolar species, with binding energy three times lower than that of NH₃. This implies that NH₃ is a more effective dangling-OH band blocker over CO₂. The reported binding energies are from Ferrero et al. (2020). The simplified geometries are an adaptation of real geometries obtained with quantum chemical calculations in Ferrero et al. (2020).

larity of a molecule, its ability to form H-bonds and to reside tightly at the dOH site, therefore impeding CO molecules from reacting with the dOH. As a general rule, we can state that polar molecules, especially NH₃ and CH₃OH, are efficient dOH blockers, whereas apolar species (e.g., CO₂) are not good dOH blockers, unless significantly more abundant than polar species, in agreement with the findings of Cuppen et al. (2011). Based on the evidence that ammonia is one of the most abundant polar species of interstellar ices after H₂O (its abundance is approximately a factor of 3 higher than that of CH₃OH; Zanchet et al. 2013; Boogert et al. 2015), we propose that in addition to the impact of thermal annealing and energetic particles, ammonia is one of the main contributors if probably not the only one in the suppression of the 2152 cm⁻¹ band, and more generally of all the dOH bands.

4.3. Other dOH-blocker candidates

The subsequent hydrogenation of N atoms leading to NH₃ at the onset of interstellar ice surfaces is not the only reaction competing with the hydrogenation of O atoms, producing dangling-OH binding sites (Hiraoka et al. 1995; Herbst & van Dishoeck 2009). For instance, the C+H reactions forming CH₄ occur concurrently with the O+H reactions (Qasim et al. 2020). This implies that CH₄ could be a good candidate for the removal or blockage of the 2152 cm⁻¹ band binding sites. However, compared to NH₃ and CO₂, CH₄ is more volatile, with similar desorption characteristics as CO (Collings et al. 2004). Laboratory studies have shown that CH₄ molecules can easily diffuse on the pore surface and do not bind to the ASW surface and hence to the dangling-OH sites tighter than CO (He et al. 2018b). We further strengthen

this argument based on the apolarity of CH₄, which in turn does not make it an efficient dOH blocker. Other species might act as suppressors of the 2152 cm⁻¹ band. Potential candidates are molecules that form onto the ices before the CO condensation stage, which steadily bind to the dOH sites because of their polarity. Examples of this class are OCN and OCS. Finally, one last category of species that could block the dOH sites are polar molecules that are produced by the interaction of CO at the dOH sites with other species present on the ice surfaces. This includes species such as H₂CO, HCOOH, and CH₃OH or even more complex organic species.

At the current stage, it is unclear whether one species contributes to the suppression of the 2152 cm⁻¹ band observed in astronomical spectra more than others, or if this is the result of multiple contributions. Further systematic laboratory experiments of ternary and quaternary mixtures are needed to constrain the composition and structure of ice mantles. In addition, quantum chemical modeling of properly mixed ices, representatives of real astronomical ices (i.e., which include at least CO, CO₂, NH₃, CH₄, and CH₃OH), may also help to elucidate the structure and spectroscopic features of the CO band, accounting for the interaction of multiple species in different H₂O-ice structural environments. Finally, high-sensitivity near- and mid-infrared observations of the dOH bands with the *James Webb Space Telescope* will provide spectra with a higher signal-to-noise ratio to compare with model predictions and experimental data.

5. Conclusions

We investigated one of the conundrums of astrochemistry: the absence of the 2152 cm⁻¹ band in observational spectra of pre-

and protostellar environments. This band is due to the interaction between CO and dangling OH bonds on the surface of water ice. By making composite ices in the laboratory that resemble the icy mantles on dust grains, we examined the impact of NH₃ and CO₂ on the 2152 cm⁻¹ band and the pore surface area of the mixed ice. We found that introducing 10% of NH₃ in ASW effectively blocks the dOH bonds as long as the ice is annealed to 100 K. At the same time, introducing NH₃ exerts only a small impact on the pore surface area of ASW. In comparison, introducing 20% of CO₂ in ASW reduces the pore surface area by half, but does block all the dOH bonds regardless of the annealing temperature. We discussed from a chemistry point of view why polar molecules such as NH₃ are likely more efficient dOH blockers than apolar molecules. We propose that NH₃ is one of the most important dOH blockers, which helps to explain the nondetection of the 2152 cm⁻¹ band, and the water-dominated layer of the ice mantle can be slightly porous, while the 2152 cm⁻¹ peak is insignificant.

6. Acknowledgements

The authors wish to thank Prof. Piero Ugliengo for the fruitful discussion on the binding energies of ammonia and carbon dioxide in interstellar ices. J.H., G.P. and T.H. acknowledge support from the European Research Council under the Horizon 2020 Framework Program via the ERC Advanced Grant Origins 83 24 28. G.V., F.E.T. and S.M.E. acknowledge support from NSF Astronomy and Astrophysics Research Grant No. 1615897.

References

- Accolla, M., Congiu, E., Dulieu, F., et al. 2011, *Physical Chemistry Chemical Physics*, 13, 8037
- Al-Halabi, A., Fraser, H. J., Kroes, G. J., & van Dishoeck, E. F. 2004, *A&A*, 422, 777
- Altwegg, K., Balsiger, H., Hänni, N., et al. 2020, *Nature Astronomy*, 4, 533
- Ayotte, P., Smith, R. S., Stevenson, K. P., et al. 2001, *J. Geophys. Res.*, 106, 33387
- Behr, P. R., Tribbett, P. D., Robinson, T. D., & Loeffler, M. J. 2020, *ApJ*, 900, 147
- Boogert, A. A., Gerakines, P. A., & Whittet, D. C. 2015, *Annu. Rev. Astron. Astrophys.*, 53, 541
- Boogert, A. C. A., Hogerheijde, M. R., Ceccarelli, C., et al. 2002, *ApJ*, 570, 708
- Boogert, A. C. A., Huard, T. L., Cook, A. M., et al. 2011, *ApJ*, 729, 92
- Boogert, A. C. A., Pontoppidan, K. M., Knez, C., et al. 2008, *ApJ*, 678, 985
- Bosman, A. D., Bruderer, S., & van Dishoeck, E. F. 2017, *A&A*, 601, A36
- Bottinelli, S., Boogert, A. C. A., Bouwman, J., et al. 2010, *ApJ*, 718, 1100
- Bu, C., Shi, J., Raut, U., Mitchell, E. H., & Baragiola, R. A. 2015, *J. Chem. Phys.*, 142, 134702
- Buch, V. & Devlin, J. P. 1991, *J. Chem. Phys.*, 94, 4091
- Chu, L. E. U., Hodapp, K., & Boogert, A. 2020, *ApJ*, 904, 86
- Collings, M. P., Anderson, M. A., Chen, R., et al. 2004, *MNRAS*, 354, 1133
- Collings, M. P., Dever, J. W., Fraser, H. J., & McCoustra, M. R. S. 2003a, *Ap&SS*, 285, 633
- Collings, M. P., Dever, J. W., Fraser, H. J., McCoustra, M. R. S., & Williams, D. A. 2003b, *ApJ*, 583, 1058
- Cuppen, H. M., Penteado, E. M., Isokoski, K., van der Marel, N., & Linnartz, H. 2011, *MNRAS*, 417, 2809
- Cuppen, H. M., van Dishoeck, E. F., Herbst, E., & Tielens, A. G. G. M. 2009, *A&A*, 508, 275
- Dartois, E., d'Hendecourt, L., Thi, W., Pontoppidan, K. M., & van Dishoeck, E. F. 2002, *A&A*, 394, 1057
- Dartois, E., Ding, J. J., de Barros, A. L. F., et al. 2013, *A&A*, 557, A97
- Dartois, E., Schutte, W., Geballe, T. R., et al. 1999, *A&A*, 342, L32
- de Graauw, T., Whittet, D. C. B., Gerakines, P. A., et al. 1996, *A&A*, 315, L345
- Devlin, J. P. 1992, *The Journal of Physical Chemistry*, 96, 6185
- D'Hendecourt, L. B. & Jourdain de Muizon, M. 1989, *A&A*, 223, L5
- Ehrenfreund, P., Boogert, A. C. A., Gerakines, P. A., Tielens, A. G. G. M., & van Dishoeck, E. F. 1997, *A&A*, 328, 649
- Ferrero, S., Zamirri, L., Ceccarelli, C., et al. 2020, *ApJ*, 904, 11
- Fraser, H. J., Collings, M. P., Dever, J. W., & McCoustra, M. R. S. 2004, *MNRAS*, 353, 59
- Fuchs, G. W., Cuppen, H. M., Ioppolo, S., et al. 2009, *A&A*, 505, 629
- Gibb, E. L., Whittet, D. C. B., Boogert, A. C. A., & Tielens, A. G. G. M. 2004, *ApJS*, 151, 35
- Goto, M., Vasyunin, A. I., Giuliano, B. M., et al. 2021, *A&A*, 651, A53
- Gürtler, J., Klaas, U., Henning, T., et al. 2002, *A&A*, 390, 1075
- He, J., Acharyya, K., & Vidalí, G. 2016, *ApJ*, 825, 89
- He, J., Clements, A. R., Emtiaz, S., et al. 2019, *ApJ*, 878, 94
- He, J., Emtiaz, S., Boogert, A., & Vidalí, G. 2018a, *ApJ*, 869, 41
- He, J., Emtiaz, S., & Vidalí, G. 2018b, *ApJ*, 863, 156
- He, J., Emtiaz, S. M., & Vidalí, G. 2017, *ApJ*, 837, 65
- Henkelman, G. & Feibelman, P. J. 2016, *The Journal of Chemical Physics*, 144, 054701
- Herbst, E. & van Dishoeck, E. F. 2009, *ARA&A*, 47, 427
- Hiraoka, K., Yamashita, A., Yachi, Y., et al. 1995, *ApJ*, 443, 363
- Ioppolo, S., van Boheemen, Y., Cuppen, H. M., van Dishoeck, E. F., & Linnartz, H. 2011, *MNRAS*, 413, 2281
- Karssemeijer, L. J. & Cuppen, H. M. 2014, *A&A*, 569, A107
- Keane, J. V., Boogert, A. C. A., Tielens, A. G. G. M., Ehrenfreund, P., & Schutte, W. A. 2001, *A&A*, 375, L43
- Kerkhof, O., Schutte, W. A., & Ehrenfreund, P. 1999, *A&A*, 346, 990
- Kimmel, G. A., Stevenson, K. P., Dohnálek, Z., Smith, R. S., & Kay, B. D. 2001, *J. Chem. Phys.*, 114, 5284
- Lauck, T., Karssemeijer, L., Shulenberger, K., et al. 2015, *ApJ*, 801, 118
- Lechner, B. A. J., Kim, Y., Feibelman, P. J., et al. 2015, *The Journal of Physical Chemistry C*, 119, 23052
- Mandell, A. M., Bast, J., van Dishoeck, E. F., et al. 2012, *ApJ*, 747, 92
- Mejía, C., de Barros, A. L. F., Seperuelo Duarte, E., et al. 2015, *Icarus*, 250, 222
- Millan, M., Teinturier, S., Malespin, C. A., et al. 2021, *Nature Astronomy*
- Mispelaer, F., Theulé, P., Aouididi, H., et al. 2013, *A&A*, 555, A13
- Mumma, M. J. & Charnley, S. B. 2011, *ARA&A*, 49, 471
- Najita, J. R., Carr, J. S., Brittain, S. D., et al. 2021, *ApJ*, 908, 171
- Noble, J. A., Dulieu, F., Congiu, E., & Fraser, H. J. 2011, *ApJ*, 735, 121
- Noble, J. A., Fraser, H. J., Aikawa, Y., Pontoppidan, K. M., & Sakon, I. 2013, *ApJ*, 775, 85
- Novozamsky, J. H., Schutte, W. A., & Keane, J. V. 2001, *A&A*, 379, 588
- Oba, Y., Miyauchi, N., Hidaka, H., et al. 2009, *ApJ*, 701, 464
- Oba, Y., Watanabe, N., Kouchi, A., Hama, T., & Pirronello, V. 2011, *Physical Chemistry Chemical Physics (Incorporating Faraday Transactions)*, 13, 15792
- Öberg, K. I., Boogert, A. C. A., Pontoppidan, K. M., et al. 2011, *ApJ*, 740, 109
- Öberg, K. I., Qi, C., Fogel, J. K. J., et al. 2010, *ApJ*, 720, 480
- Palumbo, M. E. 1997, *Journal of Physical Chemistry A*, 101, 4298
- Palumbo, M. E. 2005, in *Journal of Physics Conference Series*, Vol. 6, *Journal of Physics Conference Series*, 211–216
- Palumbo, M. E. 2006, *A&A*, 453, 903
- Palumbo, M. E., Baratta, G. A., Leto, G., & Strazzulla, G. 2010, *Journal of Molecular Structure*, 972, 64
- Palumbo, M. E. & Strazzulla, G. 1992, *A&A*, 259, L12
- Pendleton, Y. J., Tielens, A. G. G. M., Tokunaga, A. T., & Bernstein, M. P. 1999, *ApJ*, 513, 294
- Penteado, E. M., Boogert, A. C. A., Pontoppidan, K. M., et al. 2015, *MNRAS*, 454, 531
- Perotti, G., Jørgensen, J. K., Fraser, H. J., et al. 2021, *A&A*, 650, A168
- Perotti, G., Rocha, W. R. M., Jørgensen, J. K., et al. 2020, *A&A*, 643, A48
- Pontoppidan, K. M., Boogert, A. C. A., Fraser, H. J., et al. 2008, *ApJ*, 678, 1005
- Pontoppidan, K. M., Fraser, H. J., Dartois, E., et al. 2003, *A&A*, 408, 981
- Pontoppidan, K. M., Salyk, C., Banzatti, A., et al. 2019, *ApJ*, 874, 92
- Pontoppidan, K. M., Schöier, F. L., van Dishoeck, E. F., & Dartois, E. 2002, *A&A*, 393, 585
- Pontoppidan, K. M., van Dishoeck, E. F., & Dartois, E. 2004, *A&A*, 426, 925
- Qasim, D., Fedoseev, G., Chuang, K. J., et al. 2020, *Nature Astronomy*, 4, 781
- Raut, U., Famá, M., Teolis, B. D., & Baragiola, R. A. 2007a, *J. Chem. Phys.*, 127, 204713
- Raut, U., Teolis, B. D., Loeffler, M. J., et al. 2007b, *J. Chem. Phys.*, 126, 244511
- Roser, J. E., Vidalí, G., Manicò, G., & Pirronello, V. 2001, *ApJ*, 555, L61
- Rowland, B., Fisher, M., & Devlin, J. P. 1991, *J. Chem. Phys.*, 95, 1378
- Salinas, V. N., Hogerheijde, M. R., Bergin, E. A., et al. 2016, *A&A*, 591, A122
- Sandford, S. A., Allamandola, L. J., Tielens, A. G. G. M., & Valero, G. J. 1988, *ApJ*, 329, 498
- Schmitt, B., Greenberg, J. M., & Grim, R. J. A. 1989, *ApJ*, 340, L33
- Schutte, W. A. & Greenberg, J. M. 1997, *A&A*, 317, L43
- Stevenson, K. P., Kimmel, G. A., Dohnálek, Z., Smith, R. S., & Kay, B. D. 1999, *Science*, 283, 1505
- Swain, M. R., Vasisht, G., Tinetti, G., et al. 2008, *arXiv e-prints*, [arXiv:0812.1844](https://arxiv.org/abs/0812.1844)
- Watanabe, N. & Kouchi, A. 2002, *ApJ*, 571, L173
- Zamirri, L., Casassa, S., Rimola, A., et al. 2018, *MNRAS*, 480, 1427
- Zanchet, A., Rodríguez-Lazcano, Y., Gálvez, Ó., et al. 2013, *ApJ*, 777, 26
- Zhang, Q. & Buch, V. 1990a, *J. Chem. Phys.*, 92, 5004
- Zhang, Q. & Buch, V. 1990b, *J. Chem. Phys.*, 92, 1512